INTRODUCTION

The recent completion of the Graduate Aeronautical Laboratories, California Institute of Technology (GALCIT), 17-inch diameter low-pressure shock tube and its subsequent performance[1] has created a need for a pressure gauge which is capable of resolving a pressure signal on a microsecond time scale. The large diameter of the tube together with its construction as a high vacuum device has provided the researcher with a facility for generating thick near-planar[2] shock waves in rarefied gases. The advantage of thick shock waves with regard to the frequency response requirements of instruments for shock structure studies is obvious. A shock propagating with a Mach number $M_s = 7.5$ in argon at a pressure of 30 μ Hg has a pressure profile thickness of about one cm. This profile passes a fixed observer in about 5 μ sec and on reflection from a wall normal to the shock should produce a pressure-time profile on the wall with roughly the same time scale. The work being reported herein is the result of an effort to develop a suitable pressure gauge for making pressure measurements on the end wall of a shock tube for shock reflection studies on a microsecond time scale.

---

1. H. W. Liepmann, A. Roshko, D. Coles, and B.Sturtevant, Rev. Sci. Instr. 33, 625 (1962).
2. D. S. Johnson, Aero. Eng. thesis, California Institute of Technology (1962).

It should be noted that at all times we will be discussing the measurement of a pressure at a boundary and that any free stream measurement is beyond the scope of the present approach.

Of the direct methods for measuring high frequency pressure signals, the most popular and seemingly the simplest is the approach of the Hopkinson pressure bar[3] with its more recent variations[4]. The irresistible attraction of this method is the hope that a homogeneous elastic rod when struck with a uniform pressure on one end will support a plane one-dimensional wave in the axial stress σ_{xx} satisfying the well-known wave equation. That this is not true for the more interesting case where the characteristic wave length of the pressure signal is of the order of the diameter of the rod is attested by the numerous papers on the subject from Pochhammer's early work[5] (1876) to the more recent treatments of the subject[6,7].

However, this wealth of information did not dampen the enthusiasm of our initial efforts toward "developing" the pressure bar principle. After a number of unsatisfactory results, it became apparent that the "development" did not

---

3. B. Hopkinson, Phil.Trans.Roy.Soc.London 213, 437 (1914).
4. R.M.Davies, Trans.Roy.Soc. (London) 240, 375 (1948).
5. L.Pochhammer, J. angew. Math. 81, 324 (1876).
6. R. Skalak, J. Appl. Mech. 24, 59 (1957).
7. J. Miklowitz, Proc. 3rd U.S. Nat. Congr. Appl. Mech (ASME, New York, 1958), pp. 215, 224.

lie, solely, in the area of impedance matching, optically flat surfaces, and very thin bonded joints, but that the conventional pressure bar is basically quite limited by the physics of rod dynamics and by the materials available for pressure bar construction.

We propose to show that for practical limits on the variables involved the conventional pressure bar is quite unsatisfactory as a pressure measuring device on a micro-second time scale and to justify the selection of the alternate approach (a modified pressure bar) which was taken.

The variables which control the performance of a conventional pressure bar are the dimensionless ratios λ/D, x/D and ν where λ is the characteristic wave length of the pressure signal based on the elementary speed c_e ($c_e^2 = E/\rho$ where E is the Young's modulus and ρ is the density), D is the diameter of the bar, x is the distance between the front face of the bar and the axial strain sensing element, and ν is the Poisson's ratio. It is simpler to consider the case $\lambda/D = 0$ (pressure step) and to compare some characteristic quantity for the pressure bar, such as the rise time, with a similar quantity for the pressure signal to be recorded. In this case, the characteristic time D/c_e replaces the ratio λ/D as a parameter.

For $x/D \gg 1$, the effect of the Poisson's ratio on the dynamics of a rod can be accounted for, essentially, by the addition of a dispersion term to the one-dimensional wave

equation and the literature on the subject contains a number of methods for obtaining an analytical solution for the asymptotic limit. Figure 1 shows, schematically, the theoretical axial strain (an average value for the cross-section) versus time at a station many rod diameters from the end on which a pressure step is applied [8]. The first pulse is due to the dilatational wave which precedes the main bar signal because of the greater propagation velocity and which in practice is found to decay very rapidly. If τ_o is defined to be the rise time of the pressure bar, then from the above reference one can show (for $x/D \gg 1$) that the rise time scales as follows:

$$\tau_o \propto \nu^{2/3}(x/D)^{1/3}(D/c_o) . \qquad (1)$$

(The theoretical solution has been shown to give a good representation to experimental data for x/D as small as twenty[9].) From a paper by Miklowitz and Nisewanger [10] in which the measured axial strain and radial displacement versus time at various stations for a 1 in. diameter aluminum rod are presented, the value for τ_o, for $x/D = 20$, is approximately 14 μ sec. If 5 mm is selected as a practical lower limit on the diameter of a pressure bar, then using the above scaling law, while holding x/D

8. Reference 7, p. 221.

9. Reference 7, p. 222.

10. J.Miklowitz, and C.R.Nisewanger, J.Appl.Mech.24,250 (1957).

constant, one obtains a rise time of about 2.8 μ sec. This rise time would be roughly correct for most materials of interest for pressure bar construction except beryllium for which the Poisson's ratio is a factor of ten smaller and the elementary speed is a factor of two and a half larger than for these same materials. Using Eq. (1), one obtains a rise time of .24 μ sec for a 5 mm diameter beryllium rod as compared to the above value of 2.8 μ sec. If a piezoelectric material with properties matching the appropriate physical properties of beryllium was available or the pressure sensitivity requirement of the shock reflection problem was not so severe (capacitance or strain gauge principle could be used), a 5 mm diameter beryllium rod would make an excellent pressure bar for pressure signals on a microsecond time scale. However, in view of the present state of development of ceramic piezoelectric technology, this selection has to await further developments.

A scaling law for $x/D < 20$ would be mathematically very difficult to obtain from the existing literature, but at this point we can take recourse to experimental data. Figure 2(a) presents a trace for a 5 mm diameter brass rod with a .13 mm thick ceramic piezoelectric element at $x/D = .3$ which shows a rise time of about 1.4 μ sec. Both the rise time and the scale of the fluctuations in the output signal are an order of magnitude greater than that which could be tolerated for effectively displaying a pressure signal on

a microsecond time scale. A skilled craftsman could certainly construct a rod with a diameter smaller by a factor of ten, but the problem of capacitive loading of a piezoelectric element would introduce electronic complications which, if possible, should be avoided.

For x/D = 0, the behavior of the output signal changes somewhat. Figure 2(b) presents a trace for a 5 mm brass rod with a .13 mm thick ceramic piezoelectric element bonded to the front face of the rod. The rise time approaches the transit time of the pressure signal through the sensing element, but fluctuations in the output signal (due to waves generated at the corner of the rod)remain too severe to permit effective use of the bar as a pressure gauge on a microsecond time scale. In this case, it can be argued that a diameter reduction would affect only the time scale of the oscillatory fluctuations (not the amplitude of the fluctuations or the rise time of the signal) and, again, a diameter reduction of an order of magnitude would be needed to reduce the time scale of these fluctuations to an acceptable value.

As a standard of comparison for both the above results and the discussion below, the ideal pressure bar (Poisson's ratio $\nu = 0$) should be considered. In this case, the rise time would be independent of the location of the sensing element x/D and the diameter D, and the rise time would depend only on the thickness of the sensing element and the

elementary speed c_e for the material. A rough value for c_e for the ceramic piezoelectric material used in the pressure bars of Fig. 2 is 4,000 m/sec giving a rise time, for a sensing element thickness of .13 mm, of .03 μ sec. (The rise time for a good oscilloscope is $\approx$ .02 μ sec.)

The large difference between the performance of a real and an ideal pressure bar is due to the complicated three-dimensional wave motion experienced by a rod even for the apparently simple boundary conditions of a pressure bar. The desirable one-dimensional wave motion of the ideal bar can be approached in restricted regions of an elastic medium for short times and special geometries. That this can be utilized for the construction of a practical pressure gauge satisfying the requirements of sensitivity, a one-tenth microsecond rise time, and no overshoot is the subject of the following section.

APPROPRIATE GEOMETRY FOR THE PRESSURE GAUGE

Consider a rectangular coordinate system with a displacement field u, v, w as shown in Fig. 3. For simplicity, assume a rod with rectangular cross section aligned with the x axis. Let us assume that a plane wave in the displacement u = u(x, t) is propagating along the rod and see what boundary conditions are needed to permit this to occur. The strain components in the bar as computed from the displacement u(x, t) are

$$e_{xx} = \frac{\partial u(x,t)}{\partial x}$$

where the terms not listed are identically zero. The stress components then become

$$\sigma_{xx} = \frac{(1-\nu)E}{(1+\nu)(1-2\nu)} \frac{\partial u(x,t)}{\partial x}$$

$$\sigma_{yy} = \sigma_{zz} = \frac{\nu E}{(1+\nu)(1-2\nu)} \frac{\partial u(x,t)}{\partial x}$$

Shear stresses = 0.

A comparison of the lateral stresses with the axial stress shows that they must be the same functions of x and t, i.e.,

$$\sigma_{yy} = \sigma_{zz} = \frac{\nu}{(1-\nu)} \sigma_{xx} \quad . \tag{2}$$

Substituting into the non-zero component of the equilibrium

equation

$$\frac{\partial \sigma_{xx}}{\partial x} = \rho \frac{\partial^2 u}{\partial t^2} .$$

one finds

$$\frac{\partial^2 \sigma_{xx}}{\partial t^2} - c_1^2 \frac{\partial^2 \sigma_{xx}}{\partial x^2} = 0 \qquad (3)$$

where

$$c_1^2 = \frac{(1-\nu)}{(1+\nu)(1-2\nu)} \frac{E}{\rho} .$$

Equation (3) shows that the axial stress component σ_{xx} will satisfy the one-dimensional wave equation provided the normal stresses σ_{yy} and σ_{zz} are related to σ_{xx} by Eq. (2). The boundary conditions imposed by Eq. (2) are shown in Fig. 4(a). Two things become apparent. First, that the lateral stresses on the boundary must have the profile of the σ_{xx} wave and travel with it, and second, that the magnitudes of the two lateral stresses are a large fraction of the axial stress or applied pressure p(t), i.e., one half for $\nu = 1/3$.

Since the above boundary conditions would be quite difficult to satisfy in practice, without considerable development work, let us turn our attention back to a rod with a stress-free lateral surface. If the solution schematically represented in Fig. 4(b) is superposed on

the one considered in 4(a), one obtains the case of a bar with a stress-free lateral surface. The waves shown emanating from the two corners are only a schematic representation of the disturbance that must be propagating inward and it should not be assumed that a simple analytical solution is known for this case. For present purposes, a knowledge of the wave front location, which also propagates with the dilatational speed c_1, is sufficient. A detailed analysis and several example calculations on the wave system generated near the forward end of a rod by the rod impact problem can be found in a paper by Rosenfeld and Miklowitz[11].

Figure 4(c) presents the superposed stress fields, where again a rod of circular cross section and diameter D is being considered. If an imaginary rod of diameter d, within the rod proper, is imagined and if T is defined to be the time from the application of the pressure to the arrival of the first disturbance wave at the surface of the inner rod, then for the time T the inner rod will have supported the propagation of a plane one-dimensional wave in the stress σ_{xx} satisfying the wave equation. Therefore, if an element capable of sensing axial strain is inserted in the center rod, the output signal should display a rise time depending solely on the thickness of the sensing

---

11. R. L. Rosenfeld, and J. Miklowitz, Proc. 4th U.S. Nat. Congr.Appl. Mech. (ASME,New York,1962)Vol.1,pp.293,303.

element. The most efficient use of the time T can be made by moving the element forward to the front face of the rod.

Figures 5(a) and 5(b) show the geometry considered and the output for an applied step in pressure, respectively. Two features of the present geometry should be noticed. The extremely short rise time τ associated with the element thickness h and the dilatational speed c_1 is obtained, and the characteristic oscillations (due to the longitudinal and possible radial modes associated with the Pochhammer frequency equation for the rod) are absent from the output signal for the duration of the dwell time T. The dwell time T depends on the distance (D-d)/2 and the dilatational speed c_1. It is obvious that the price paid for the ideal behavior is a limit on the useful time of the gauge, i.e., the dwell time T, and the gauge diameter D has to be somewhat larger than that experienced with conventional bars. The increased diameter also necessitates a larger source of uniform pressure for recording a pressure signal. For shock tube flows, this restricts the application of the gauge to end wall pressure measurements and eliminates its application to side wall measurements.

SENSING ELEMENT

The primary considerations involved in the selection of a sensing element are the following: (1) the rod must be a homogeneous elastic medium and care must be taken to match the acoustic impedance of the sensing element to that of the rod; (2) the output of the sensing element must be reasonable for the pressure measurement level entertained; (3) the dilatational speed c_1 has to be compatible with the desired dwell time and any limit on the gauge diameter. Also, since there are many subtle problems associated with the actual construction of any gauge, the sensing element chosen will certainly depend on the set of problems the designer cares to handle.

The pressure gauge on which we are reporting was designed to record the pressure profile of a reflecting shock wave on the end wall of the GALCIT 17-in.low-pressure shock tube. The gauge rod diameter was limited to 1 3/8 in. because, first, that was the size of the available holes in the end plate of the shock tube; and, second, because of shock curvature it was decided to limit the gauge diameter to a portion of the shock surface that could be considered flat. Figure 6 presents the measured curvature[12] of the shock surface at the instant of reflection of the shock from the end wall, as a function of initial pressure p_1 and the radial position r/R. The indicated

12. Reference 2, p. 85.

shock pressure profile thicknesses were obtained by using an average value of three mean free path lengths (based on the initial pressure) for the shock thicknesses. A comparison of the curvature, at the outer radius of the gauge, to the shock thickness shows that the curvature is about 0.5 per cent of the shock thickness, for the pressure range given by the data.

The sensing element used was based on the capacitor gauge principle and the rod was constructed of polycarbonate plastic. This selection gave a dwell time of 5 μ sec which is twice that which can be obtained with a piezoelectric element and an appropriate rod material (for the same 1 3/8 in. gauge diameter). Although the present selection seems to be the better, in view of the longer dwell time and the results of the experimental data to be presented, had ceramic piezoelectric material in the form of large plates been available during the development phase, it certainly would have been tried.

Figure 7 shows schematically the features of the present design. The capacitance formed by the inner and outer electrodes C_o is changed by a small amount ΔC during propagation of a strain wave in the rod and this capacitance change is converted into an electrical signal by the circuit shown in Fig. 8(a). An analysis of the circuit shows that the output $\Delta V(t)$ (across the resistance R) for a step change in capacitance of ΔC is given by

Fig. 8(b). Since the useful time of the gauge is limited by the dwell time, the RC_o decay of the signal, shown in the figure, is not a very serious matter and considerable simplicity is gained over the standard bridge circuitry for a capacitance gauge and the associated 20 megacycle frequency generator that would be needed in this case. The RC_o decay time is 100 μ sec for the present design which yields a 5 per cent decay of the signal after 5 μ sec.

Converting the quantity $\Delta C/C_o$ into a strain and then expressing it in terms of a pressure jump ΔP and the Young's modulus of the dielectric material E, we have from Fig. 8(b)

$$\Delta V = \frac{V}{E} \Delta P \ . \qquad (4)$$

One of the nice features of a capacitance gauge with the above circuit is that the decay time, which is not critical, depends on the value of the capacitance C_o which is very difficult to control since the electrode separation h is such a small dimension. The amplitude of the output, however, depends on items easy to control (from gauge to gauge and run to run), i.e., the applied voltage V and the Young's modulus of the dielectric material E. The sensitivity of the gauge is then the ratio V/E and is the quantity that has to be maximized when sensitivity is important. The sensitivity V/E is somewhat smaller than that estimated from handbook data. The dynamic modulus

of polycarbonate plastic, for the strain rates imposed by the operation of the gauge, is five times larger than the listed value[13]. (This is not at all unusual for a polymer plastic experiencing a strain rate of the order of 100 in./in./sec.) Also, a practical limit on the applied voltage is 30 per cent of the dielectric strength of the material since small current discharges become more frequent and severe as the breakdown voltage is approached.

---

13. Modern Plastics Encyclopedia Issue for 1962 (Plastics Catalogue Corp., Bristol, Conn., 1961), Vol. 39,p.373.

GAUGE CONSTRUCTION

Figure 9 shows the gauge assembly presently being used. The translucent material is Lexan (General Electric's polycarbonate plastic) and the transparent material is Lucite (DuPont's acrylic plastic). The Lucite rods (one of the materials tested) are presented to show the internal construction of the gauge, whereas, the Lexan is being used because of its greater dielectric strength.

The Lexan rod was first machined to size and appropriate holes drilled. The front face was hand ground (with a Lexan block, grinding compound and water) in three stages ending with #800 grit grinding compound. Eccobond 57C conducting epoxy (Emerson and Cumming, Inc.) was then used to form the center conductor and the internal electrode. After thorough setup of the epoxy (24 hours at 80°C), the front face was reground with #800 grit grinding compound until the thickness of the electrode had been reduced to the point where a strong light would only begin to show through the electrode. (If the electrode is ground too thin, more epoxy can be added and the operation repeated.) A disk of Lexan (1½ in. in diameter and 3/16 in. thick) of which one face had been ground flat was then cemented to the Lexan rod. Best bonding results were obtained with a very thin coat of Adweld (Miracle Adhesive Corp.) applied to both surfaces

and then held together under a moderate pressure for 24 hours at room temperature. (Heat is not recommended at this point because greater internal stresses would be introduced and it would take longer for the stresses to relax.) Methylene chloride which is suggested in the literature for solvent bonding of polycarbonate plastic was found to be much too active and was discarded. The disk was then turned down on a lathe to the proper diameter and to twice the final thickness. Final sizing of the disk to .005 in. in thickness was done with kerosene and sandpaper (#320 and #600 grit) on a marble flat, then ground with #800 grit grinding compound as above. Of course, an appropriate guide block was used in all stages of grinding. A very thin coating of electrical grade silver paint, shown in Fig. 9, was then applied with an air brush to form the outer electrode and contact to ground and the front face was again reworked to make a smooth surface on the silver paint. (A paint brush cannot be used to apply the coating because toluene, the solvent in silver paint, softens Lexan quite rapidly.) After assembly with the holder, a couple of dabs of silver paint completed the electrical contact between the outer electrode and ground.

GAUGE PERFORMANCE

Ideally one would like to apply a step in pressure to the gauge to check the rise time, the dwell time, and the RC_o decay against the above calculations. Assuming proper conditions, the shock tube is probably the best source for a pressure step on a microsecond time scale. Figure 10 shows the response of the gauge when mounted flush with the end wall of the GALCIT 17-in. shock tube and for a shock Mach number M_s of 1.20 in air at an initial pressure p_1 of 400 mm Hg. The figure shows a dwell time of about 5 μ sec and a rise time of about 0.1 μ sec. The RC_o decay seems to be about 5 per cent. A slight rounding of the upper corner can be seen in the figure and, at this stage, it is felt that this is due to heat transfer to the end wall which is reducing the pressure behind the reflected shock for a short time. This conclusion was drawn because of the more pronounced effect at p_1 = 1.5 mm Hg, Fig. 11, where the shock thickness is still too thin to be resolved by the pressure gauge but the density has been reduced to a value where the heat transfer effect should be greater. Figures 12 through 16 show the thickening of the pressure profile on the end wall due to a reflecting shock with increasing shock Mach number and decreasing pressure. Two things should be noted with regard to the figures. First, that the grid is distorted at the edges of the oscillogram and, second, that the more sensitive

settings of Figs. 15 and 16 show a slight slope in the zero ordinate before the shock arrives and this should not be confused as being part of the pressure profile.

Figure 17 presents the calibration of the gauge. The jump in voltage was measured from a number of traces and plotted against the theoretical pressure jump for a known shock Mach number and initial pressure. The shock Mach number was measured 45 cm upstream of the end wall by measuring the transit time of the shock between two thin film heat gauges in the side wall of the shock tube 50 cm apart on a microsecond counter. An amplifier with an amplification of 30X was used between the pressure gauge and the Tektronix 555 dual beam oscilloscope used to display the traces. The voltage jumps plotted in Fig. 17 are the voltages appearing across the 1M grid resistor (without the 30X amplification) and normalized to a common gauge voltage of 4 kV. The sensitivity of the gauge V/E as read from the figure is 56 μv/mm Hg. Converting the sensitivity back into a number for E, we obtain a value five times greater than the listed value for the Young's modulus of polycarbonate plastic, as noted above.

In view of the response of the gauge to a step in pressure, Fig. 10, and the linearity exhibited by the calibration curve, Fig. 17, the pressure traces, Figs. 12 through 16, must surely be good representations of the actual pressure histories on the end wall of the shock

tube for the quoted conditions. To our knowledge, this is the first reported instance of pressure measurements having been made for reflecting shock waves showing the details of the pressure profiles on the boundary. The gauge originally was specifically designed to make measurements of this type. But with the present experience on the construction and performance of this type of gauge and the data on shock reflection that the gauge has made available, there are now several additional exciting possibilities open for investigation, one of these being the question of the effect of heat transfer to the end wall on the pressure behind a reflected shock mentioned above. Some investigations in this area are presently underway and will be reported in a forthcoming paper.

Of course, for some regions of investigation a modification to the present gauge may be necessary, such as increasing the dwell time or decreasing the rise time. But the basic gauge principle would remain the same. The diameter of the gauge could certainly be increased to raise the dwell time to 10 μ sec and still have a reasonable ratio of shock curvature to shock thickness over the surface of the gauge for a large diameter shock tube such as the GALCIT 17-in. shock tube. An alternative to increasing the gauge diameter would be to try to greatly reduce or even eliminate the disturbance arriving from the free boundary by encasing the rod in a lead jacket, somewhat

similar to what is done for an ultrasonic delay line where each crystal is backed with a lead absorber to eliminate the "echo" from the free boundary of the crystal.

For a gauge with a still shorter rise time and for the case where the thickness of the sensing element could not be reduced (limited by sensitivity), a piezoelectric material with its greater dilatational speed should be considered. The selection of a piezoelectric material would have to be limited to the ceramic type which can be locally polarized. This would be necessary because the gauge construction would require the use of a single piezoelectric disk of diameter D, whereas the active region has to consist of a smaller disk of diameter d. Suitable electrodes would have to be provided for the locally polarized region to keep the excess capacitance to a minimum, because excess capacitance reduces the output from a piezoelectric element. Some obvious practical difficulties would arise in trying to provide suitable electrodes. But, assuming the problems could be overcome, a gauge with a rise time of .03 μ sec and no overshoot seems quite reasonable now, using a.13 mm thick ceramic piezoelectric disk bonded to a brass rod.

The gauge design is not limited to shock tube work and may also be useful in measuring pressure jumps for detonation work in gases and shock waves in liquids or for almost any application where the accurate arrival time of

a pressure pulse traveling in a direction normal to the plane of the gauge is needed. For MHD studies with electromagnetically driven shocks, information on the existence of a pressure jump, its magnitude, and arrival time could be obtained with the gauge, with a minimum of electrical interference from the arc discharge. (The outer electrode would provide a reasonable amount of shielding for the gauge.) Also, by using the gauge principle, the dynamic modulus of various dielectric materials for very large strain rates could be measured by noting the sensitivity V/E for each gauge made of these various dielectric materials.

ACKNOWLEDGMENTS

The author is deeply indebted to Professors H. W. Liepmann and A. Roshko for suggesting the study of the shock reflection problem and for their guidance and continual encouragement during the investigation. Very informative discussions with Professor J. Miklowitz on the subject of wave propagation in a rod and with Dr. R. Ashby of the Autonetics Division of North American Aviation, Inc., on the construction practices for ultrasonic delay lines were extremely helpful towards the successful completion of the present investigation and are also gratefully acknowledged.

The testing conducted in the GALCIT 17-in. low-pressure shock tube was supported by the National Aeronautics and Space Administration.

LIST OF FIGURES

Fig. 5. (a) Geometry of the pressure gauge. (b) A diagrammatic representation of the output of the axial strain sensing element for a short time after the application of a pressure step. The rise time τ is given by h/c_1 and the dwell time T by $(D-d)/2c_1$.

Fig. 6. The measured curvature of the shock wave surface (from Ref. 2) as a function of radial position r/R and initial pressure p_1 for the GALCIT 17-in. low-pressure shock tube.

Fig. 7. A schematic drawing of the pressure gauge showing the construction of the capacitor type sensing element.

Fig.8. (a) Sensing element circuit. (b) Voltage output $\Delta v(t)$ for a step change in capacitance ΔC of the sensing element capacitor C_o provided $\Delta C/C_o \ll 1$.

Fig.9. Pressure gauge assembly and example rod elements.

Fig. 10. The response of the pressure gauge to the pressure step produced by a reflected shock where:

Incident shock Mach no.: $M_s = 1.20$
Driven gas: Air at 400 mm Hg
Pressure jump: $\Delta P = 496$ mm Hg
Gauge voltage: V = 1.5 kV
Upper trace: .10 v/cm, 1 μ sec/cm
Lower trace: .50 v/cm, 10 μ sec/cm

Fig. 11. The effect on the pressure behind a reflected shock due to heat transfer to the shock tube end wall. The test conditions were:

Incident shock Mach no.: $M_s = 5.05$
Driven gas: Argon at 1.5 mm Hg
Pressure jump: $\Delta P = 246$ mm Hg
Gauge voltage: V = 3.0 kV
Upper trace: .10 v/cm, 1 μ sec/cm
Lower trace: .50 v/cm, 5 μ sec/cm

Fig. 12. Pressure profile due to a reflecting shock where the incident shock thickness is greater than the resolution of the pressure gauge. The test conditions were:

Incident shock Mach no.: $M_s = 5.85$
Driven gas: Argon at 500 μ Hg
Pressure jump: $\Delta P = 114$ mm Hg
Gas voltage: V = 1.6 kV
Upper trace: .05 v/cm, 1 μ sec/cm
Lower trace: .20 v/cm, 5 μ sec/cm

Fig. 13. Pressure profile for a reflecting shock wave where:

Incident shock Mach no.: $M_s = 6.37$
Driven gas: Argon at 200 μ Hg
Pressure jump: $\Delta P = 55.2$ mm Hg
Gauge voltage: V = 4.0 kV
Upper trace: .05 v/cm, 1 μ sec/cm
Lower trace: .01 v/cm, 5 μ sec/cm

Fig. 14. Pressure profile for a reflecting shock wave where:

Incident shock Mach no.: $M_s = 6.65$
Driven gas: Argon at 100 μ Hg
Pressure jump: $\Delta P = 30.5$ mm Hg
Gauge voltage: V = 4.0 kV
Upper trace: .05 v/cm, 1 μ sec/cm
Lower trace: .10 v/cm, 5 μ sec/cm

Fig. 15. Pressure profile for a reflecting shock wave where:

Incident shock Mach no.: $M_s = 7.00$
Driven gas: Argon at 50 μ Hg
Pressure jump: $\Delta P = 17.4$ mm Hg
Gauge voltage: V = 4.0 kV
Upper trace: .02 v/cm, 1 μ sec/cm
Lower trace: .10 v/cm, 5 μ sec/cm

Fig. 16. Pressure profile for a reflecting shock wave where:

Incident shock Mach no.: $M_s = 7.40$
Driven gas: Argon at 30 μ Hg
Pressure jump: $\Delta P = 11.8$ mm Hg
Gauge voltage: V = 4.0 kV
Upper trace: .02 v/cm, 1 μ sec/cm
Lower trace: .05 v/cm, 5 μ sec/cm

Fig. 17. Gauge calibration showing the output voltage jump versus the theoretical pressure jump across a reflected shock for a known shock Mach number and initial pressure.

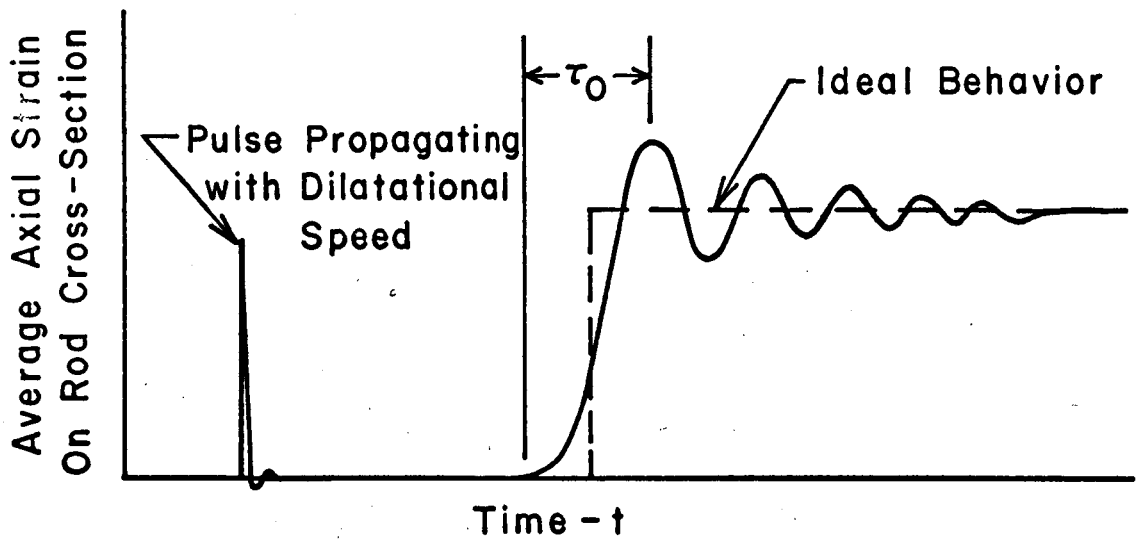

FIG. 1.
D. BAGANOFF
REV. SCI. INSTR.

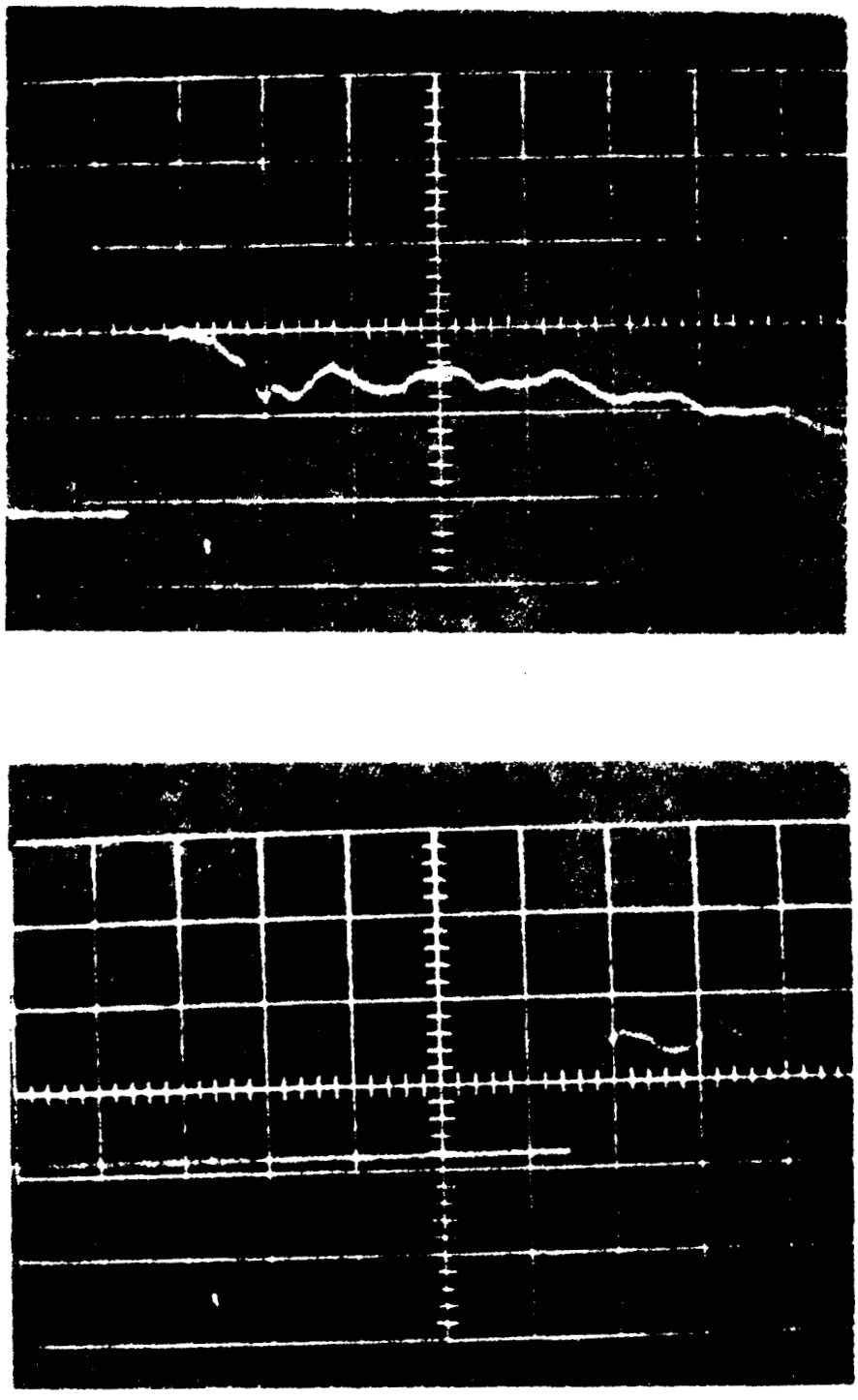

(b)

Fig. 2. The response of a 5 mm diameter brass rod to a pressure step. (a) A .13 mm thick ceramic piezoelectric element was located at a station x/D = .3. (b) A .13 mm thick ceramic piezoelectric element was located on the front face of the rod. In each case the sweep speed of the oscilloscope was 2 μ sec/cm.

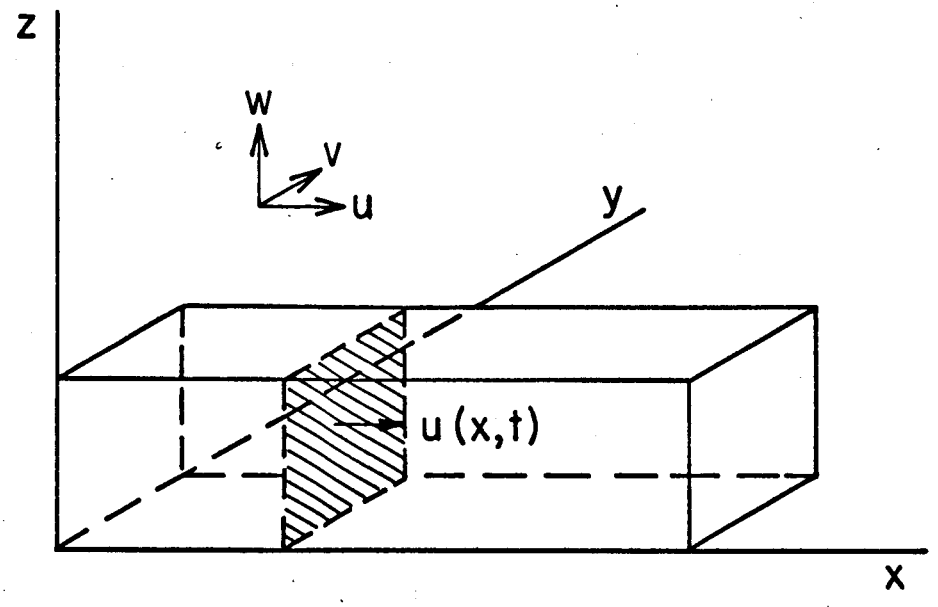

FIG. 3.
D. BAGANOFF
REV. SCI. INSTR.

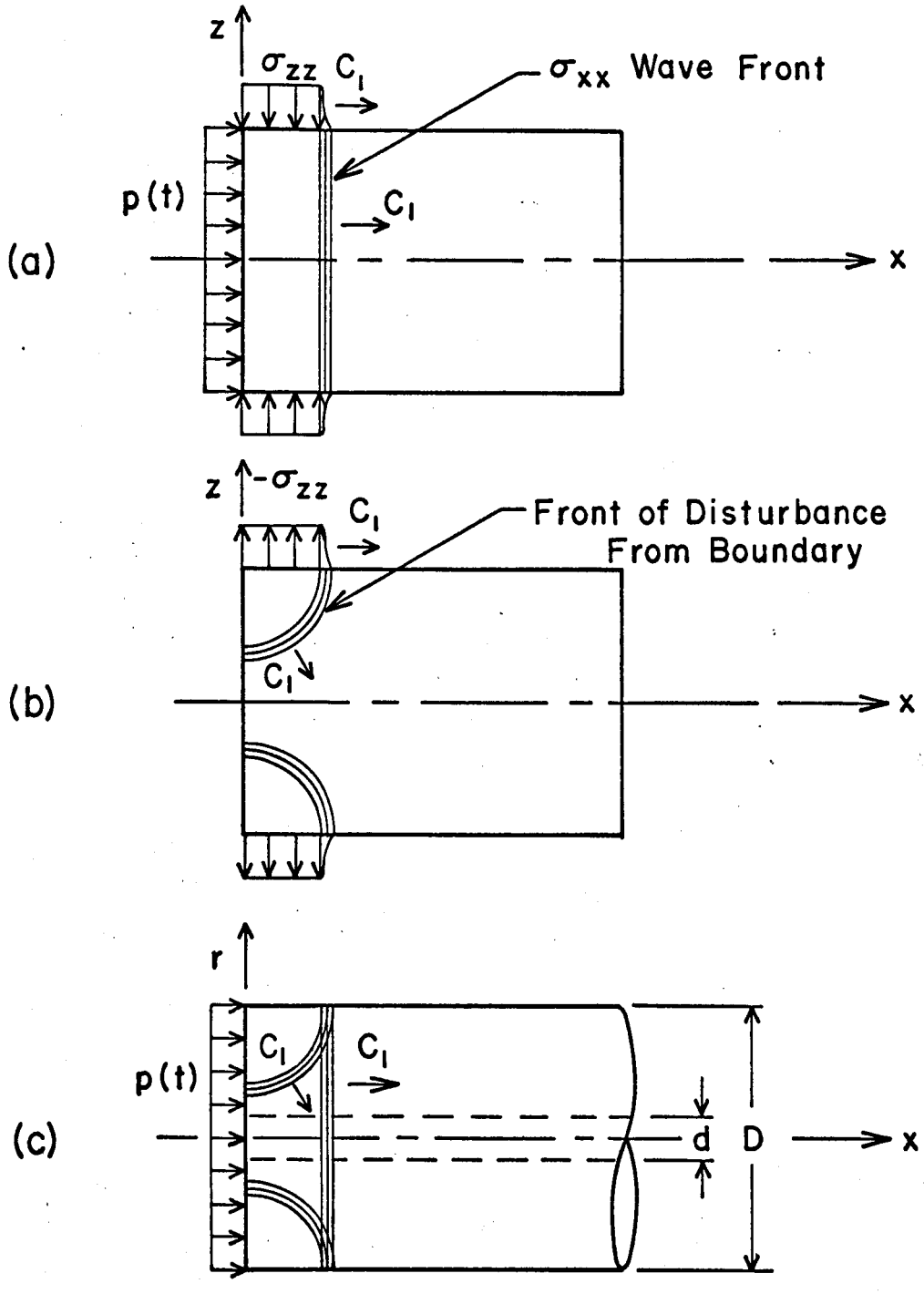

FIG. 4.
D. BAGANOFF
REV. SCI. INSTR.

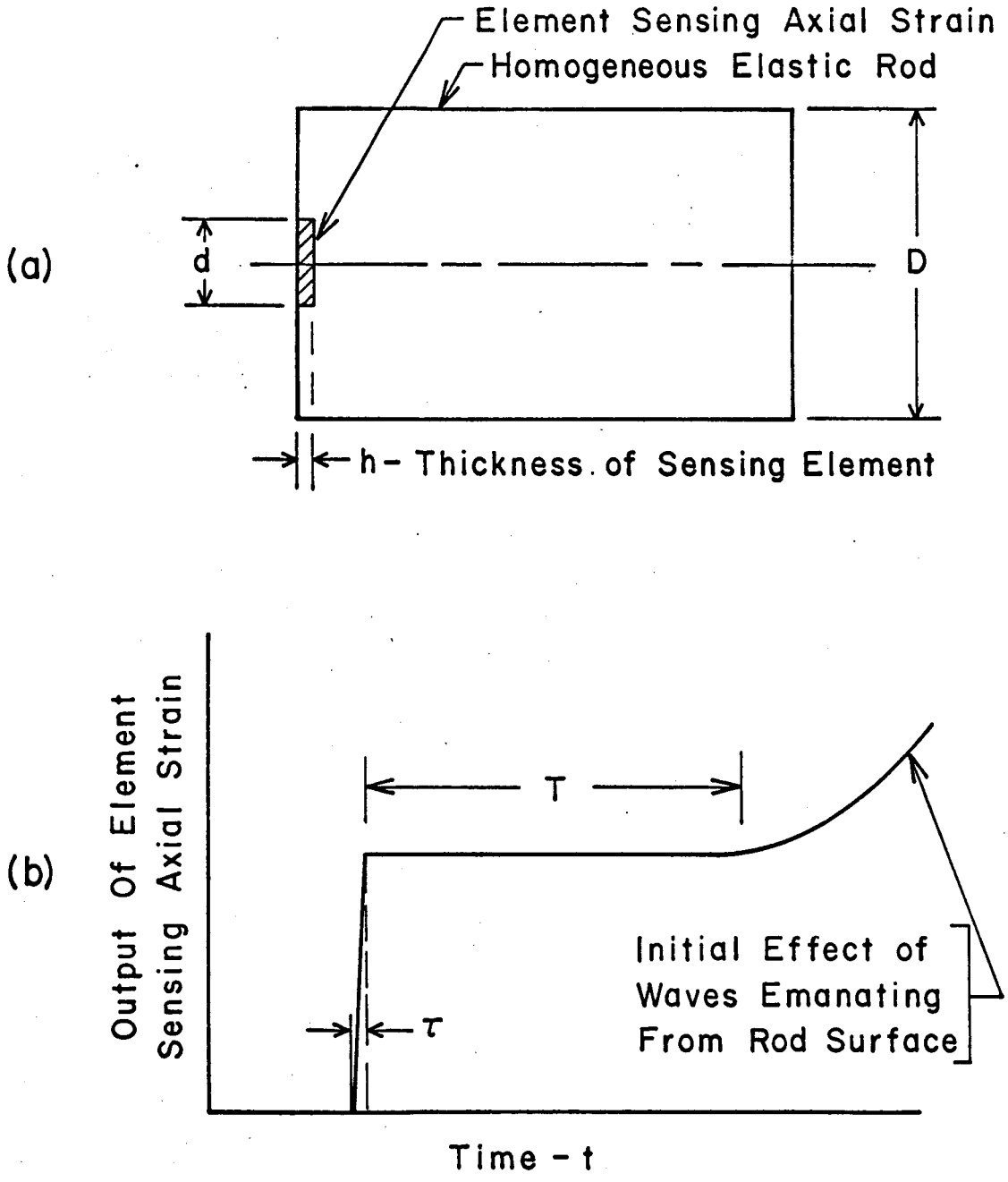

FIG. 5.
D. BAGANOFF
REV. SCI INSTR.

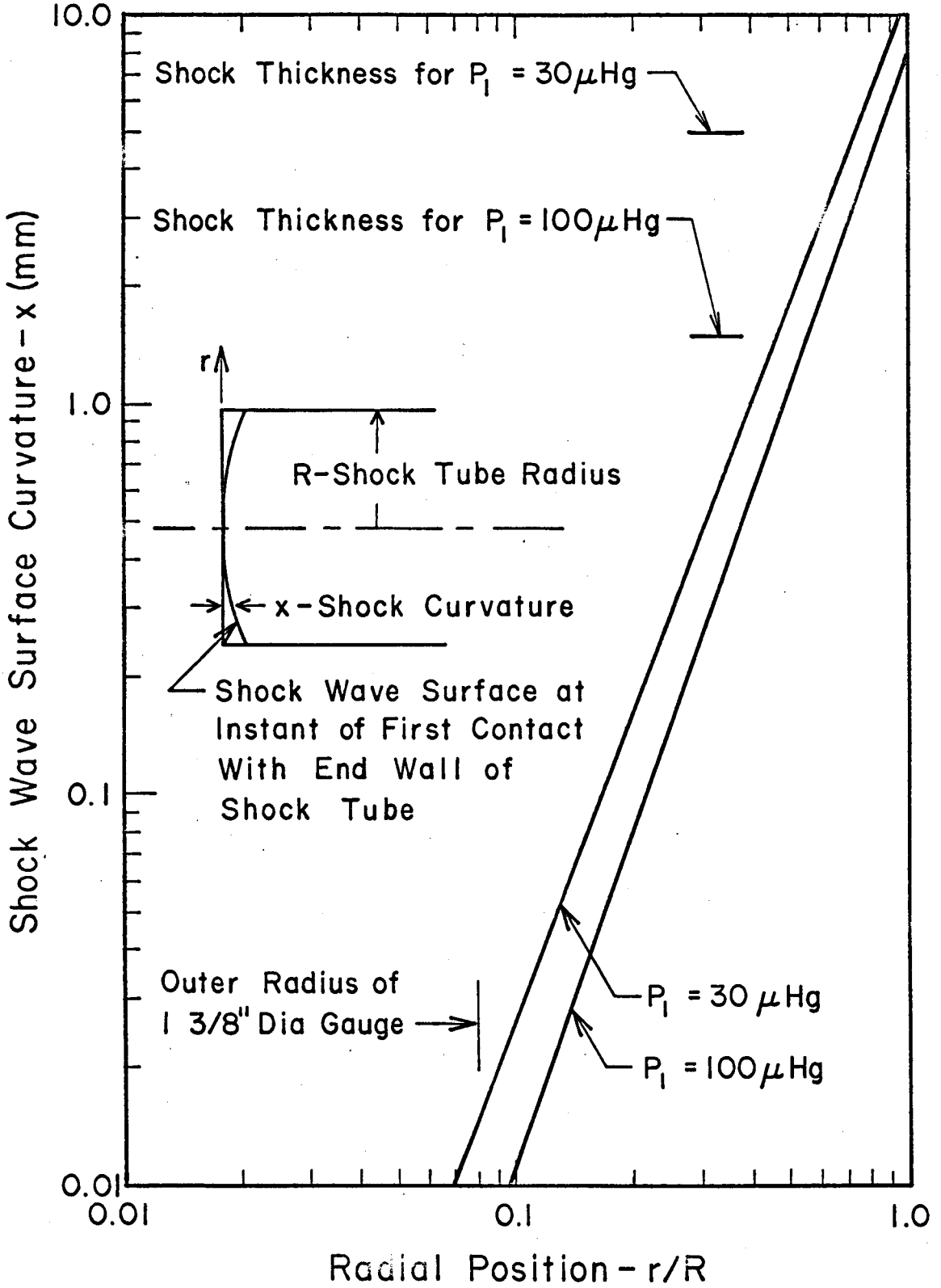

FIG. 6.
D. BAGANOFF
REV. SCI. INSTR.

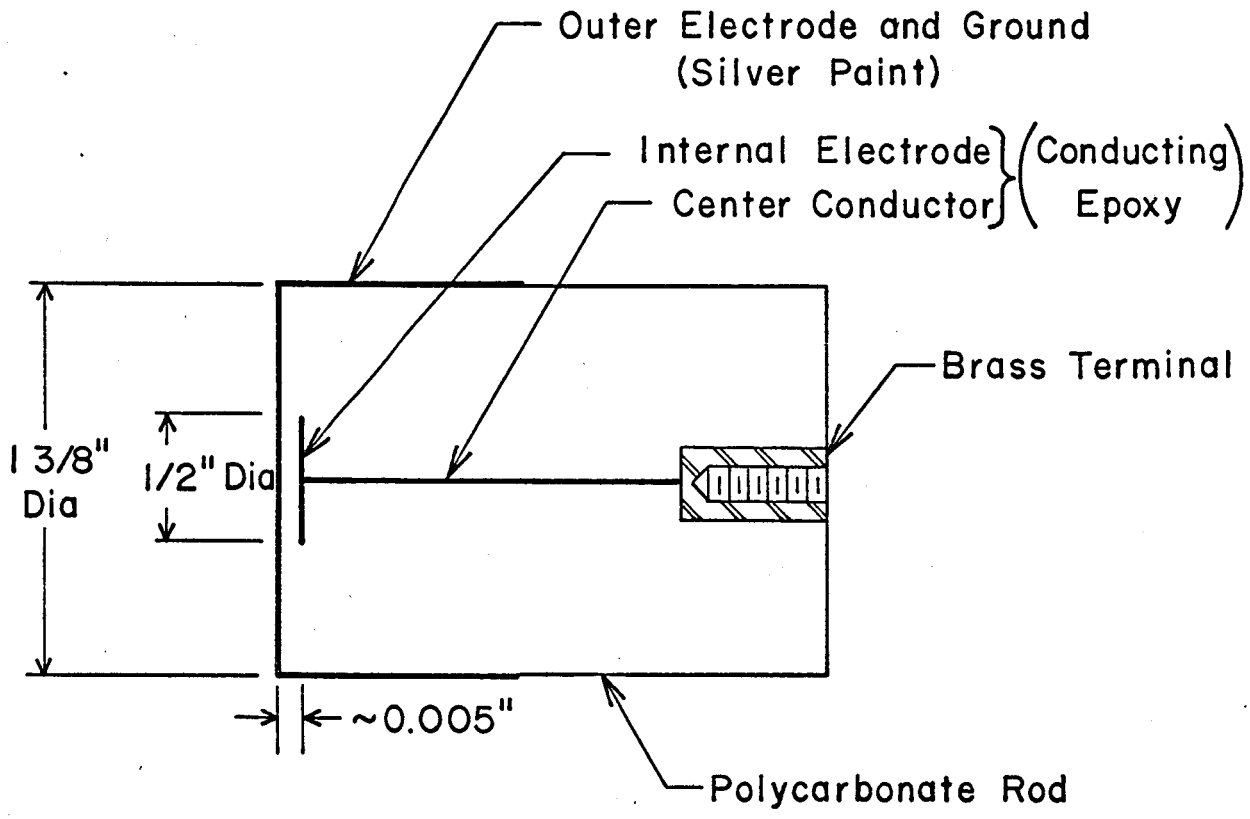

FIG. 7.
D. BAGANOFF
REV. SCI. INSTR.

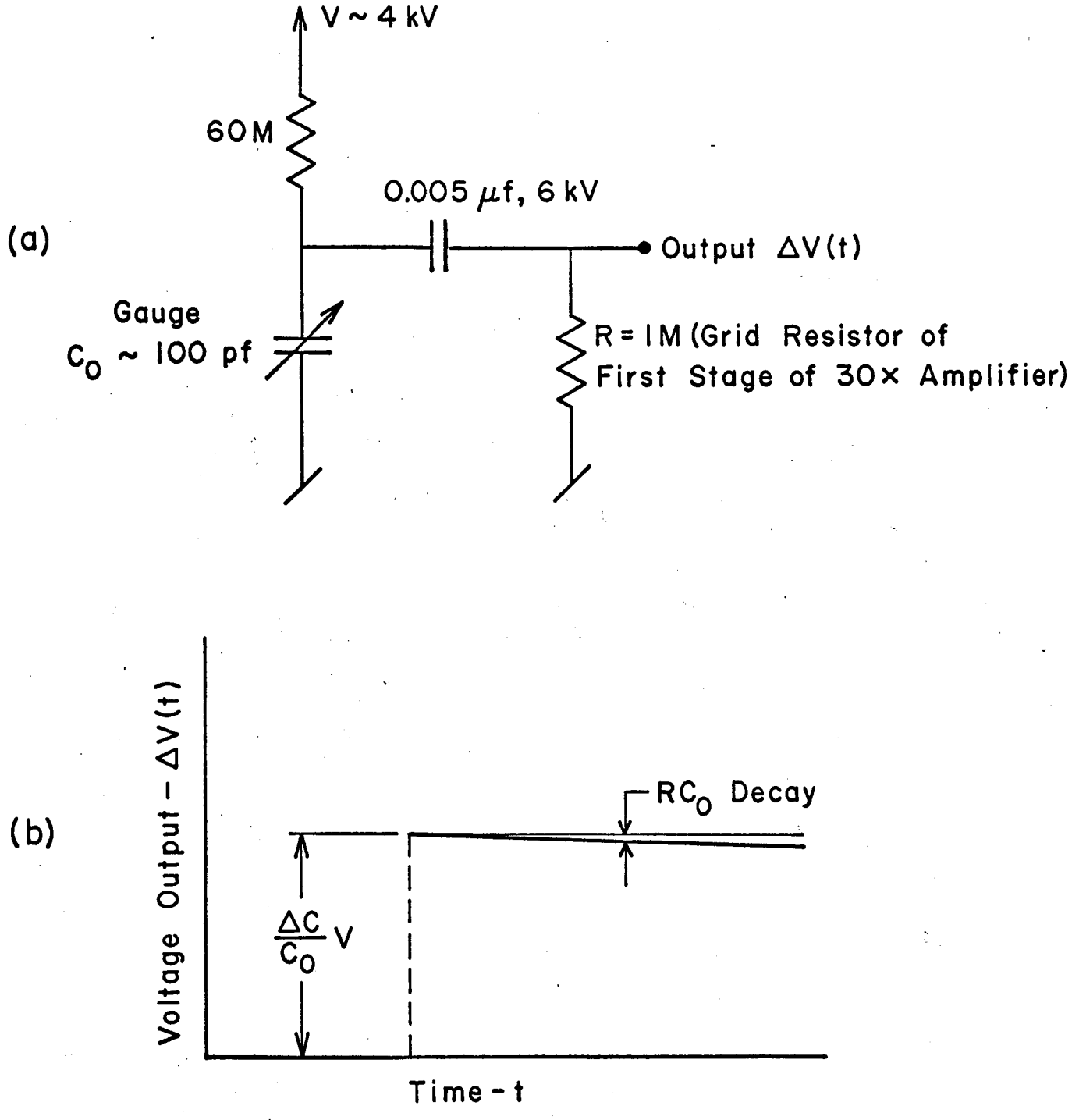

FIG. 8.
D. BAGANOFF
REV. SCI. INSTR.

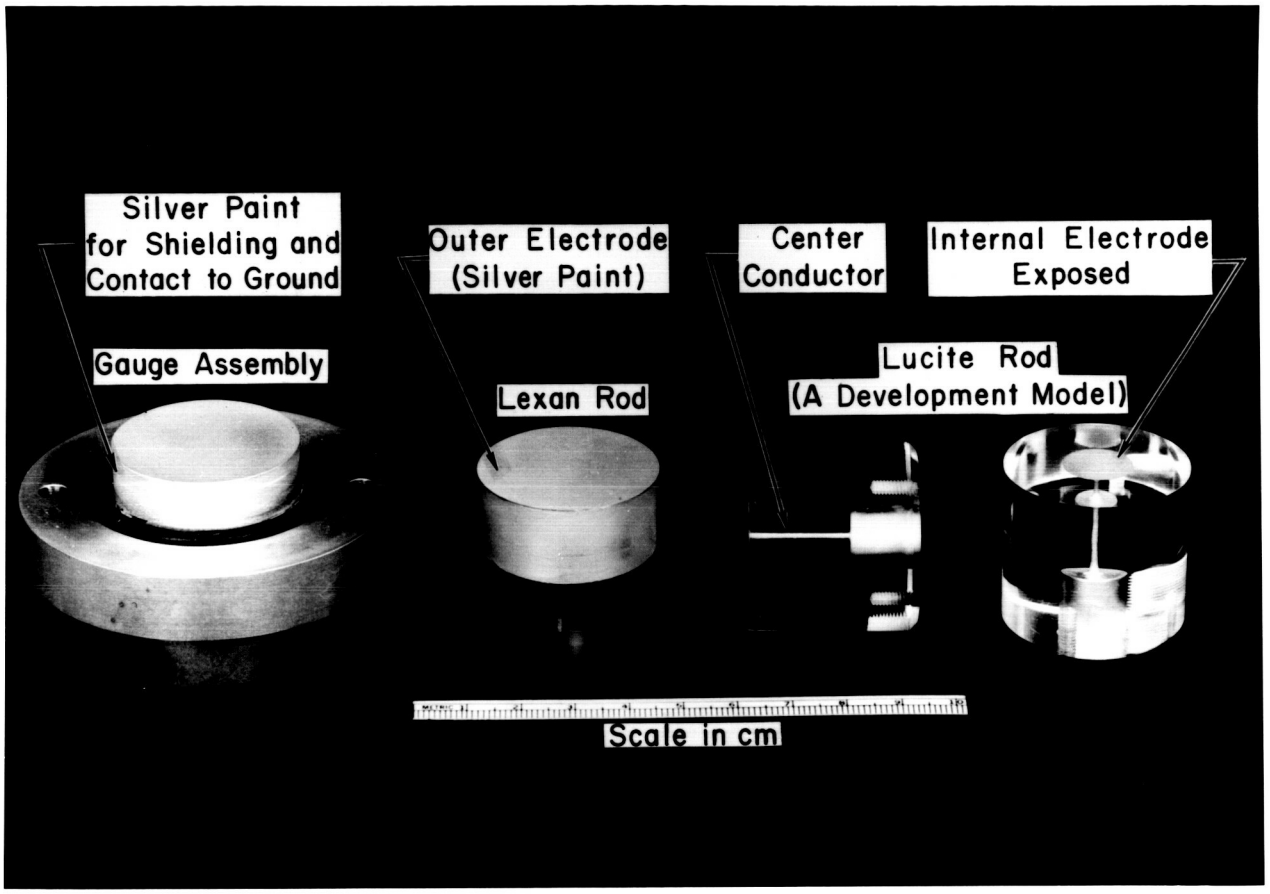

Fig. 9. Pressure gauge assembly and example rod elements.

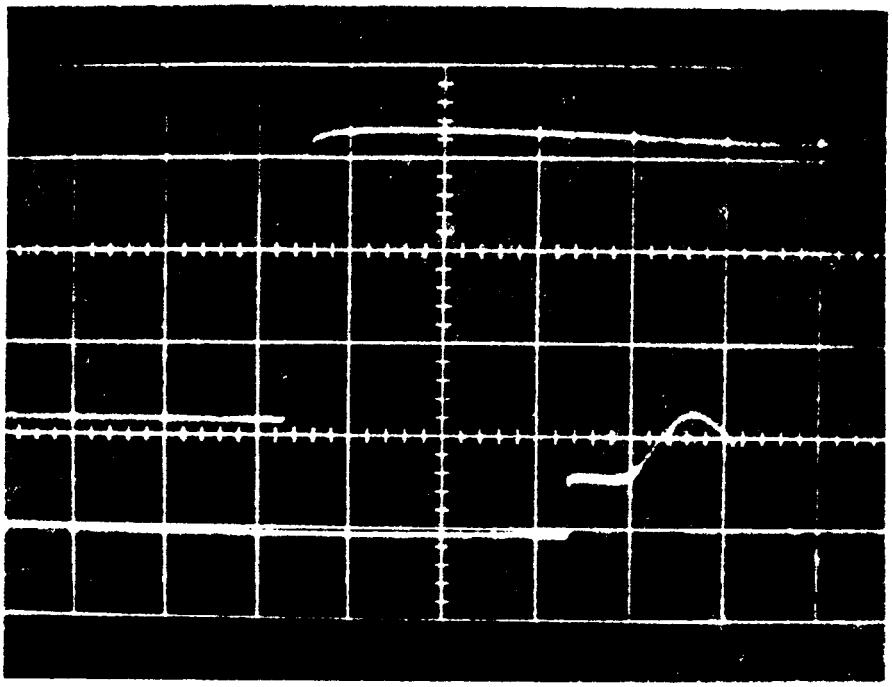

Fig. 10. The response of the pressure gauge to the pressure step produced by a reflected shock where:

Incident shock Mach no.: $M_s = 1.20$
Driven gas: Air at 400 mm Hg
Pressure jump: $\Delta P = 496$ mm Hg
Gauge voltage: V = 1.5 kV
Upper trace: .10 v/cm, 1 μ sec/cm
Lower trace: .50 v/cm, 10 μ sec/cm

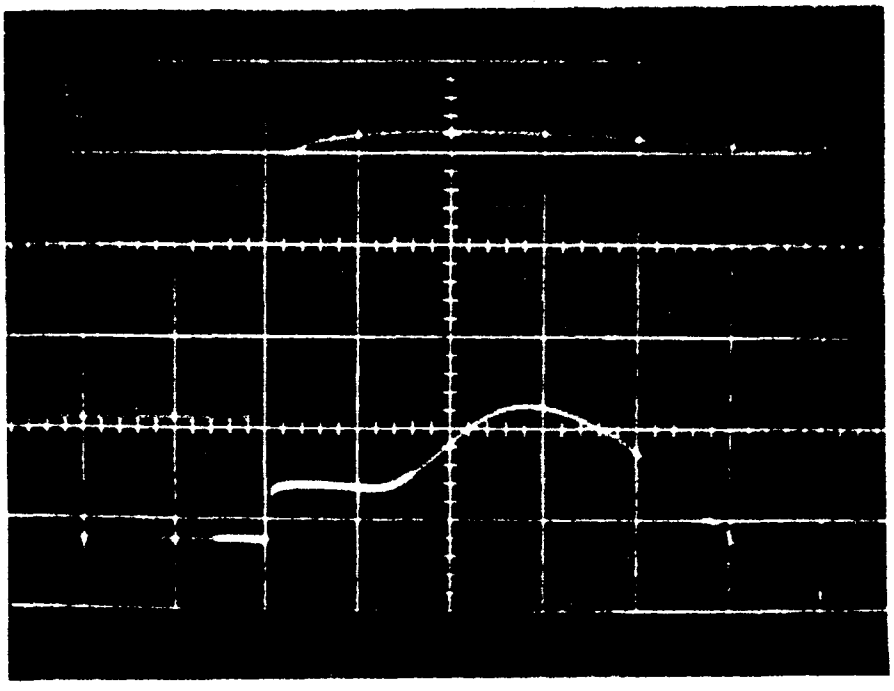

Fig. 11. The effect on the pressure behind a reflected shock due to heat transfer to the shock tube end wall. The test conditions were:

Incident shock Mach no.: $M_s = 5.05$
Driven gas: Argon at 1.5 mm Hg
Pressure jump: $\Delta P = 246$ mm Hg
Gauge voltage: V = 3.0 kV
Upper trace: .10 v/cm, 1 μ sec/cm
Lower trace: .50 v/cm, 5 μ sec/cm

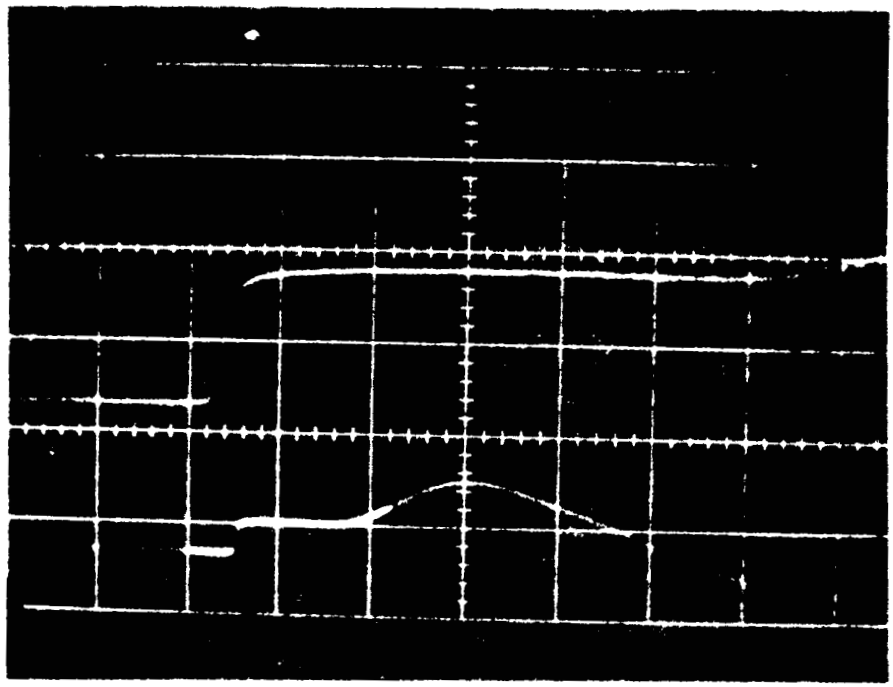

Fig. 12. **Pressure profile due to a reflecting shock wave where the incident shock thickness is greater than the resolution of the pressure gauge.** The test conditions were:

Incident shock Mach no.: $M_s = 5.85$
Driven gas: Argon at 500 μ Hg
Pressure jump: $\Delta P = 114$ mm Hg
Gas voltage: V = 1.6 kV
Upper trace: .05 v/cm, 1 μ sec/cm
Lower trace: .20 v/cm, 5 μ sec/cm

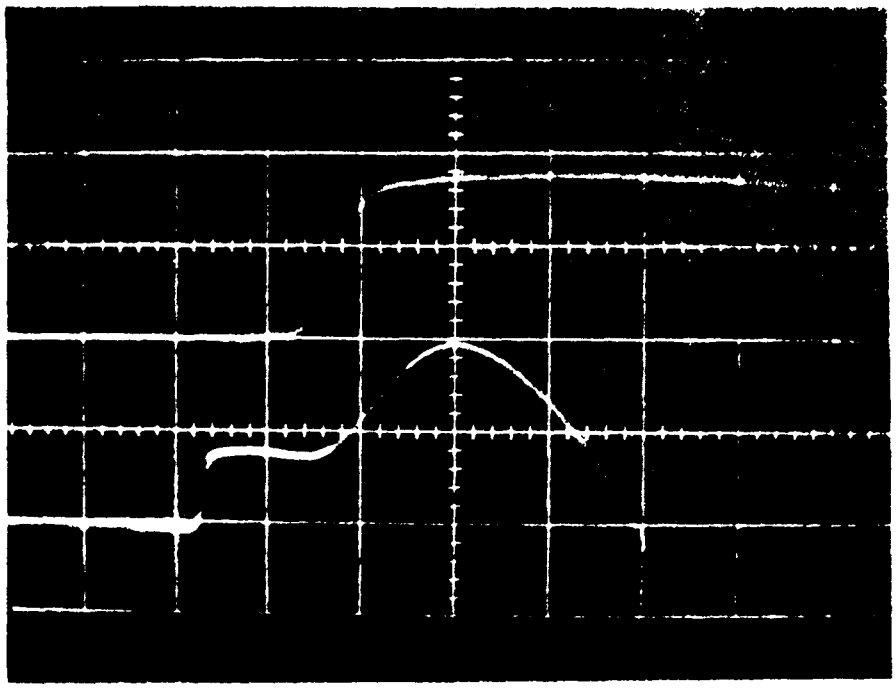

Fig. 13. Pressure profile for a reflecting shock wave where:

Incident shock Mach no.: $M_s = 6.37$
Driven gas: Argon at 200 μ Hg
Pressure jump: $\Delta P = 55.2$ mm Hg
Gauge voltage: V = 4.0 kV
Upper trace: .05 v/cm, 1 μ sec/cm
Lower trace: .01 v/cm, 5 μ sec/cm

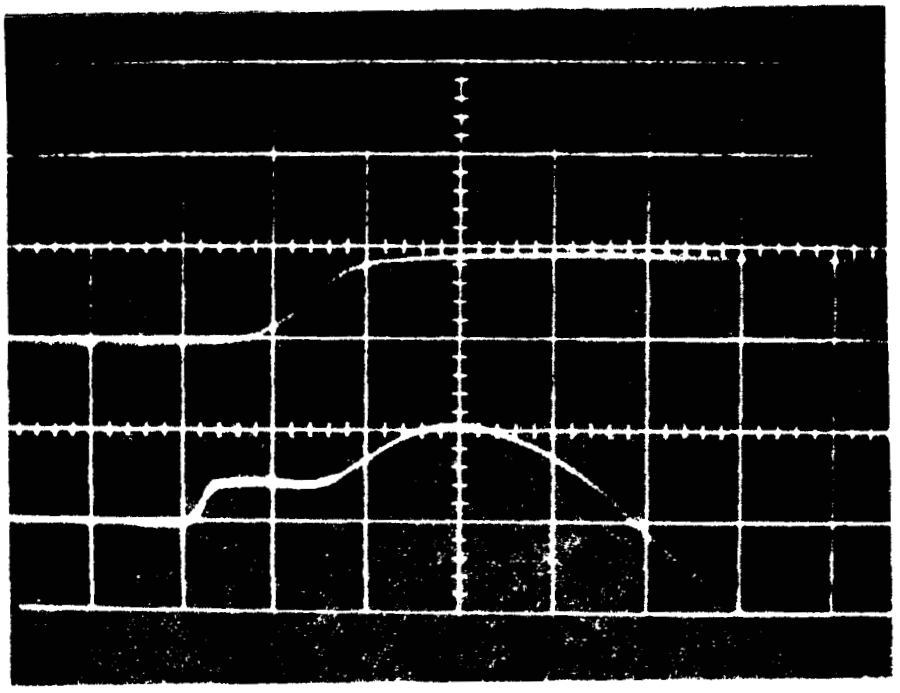

Fig. 14. Pressure profile for a reflecting shock wave where:

Incident shock Mach no.: $M_s = 6.65$
Driven gas: Argon at 100 μ Hg
Pressure jump: $\Delta P = 30.5$ mm Hg
Gauge voltage: V = 4.0 kV
Upper trace: .05 v/cm, 1 μ sec/cm
Lower trace: .10 v/cm, 5 μ sec/cm

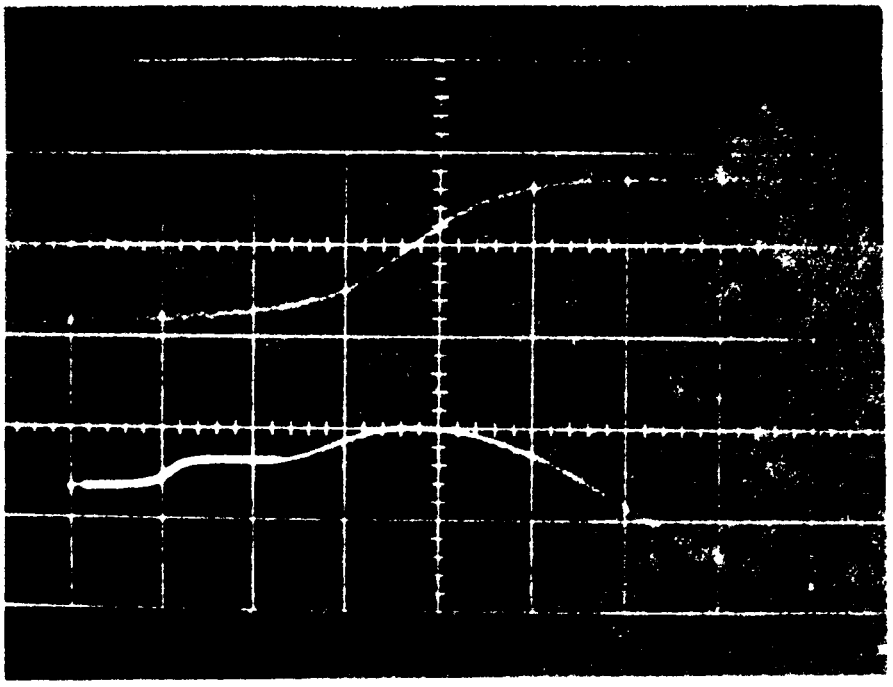

Fig. 15. Pressure profile for a reflecting shock wave where:

Incident shock Mach no.: $M_s = 7.00$
Driven gas: Argon at 50 μ Hg
Pressure jump: $\Delta P = 17.4$ mm Hg
Gauge voltage: V = 4.0 kV
Upper trace: .02 v/cm, 1 μ sec/cm
Lower trace: .10 v/cm, 5 μ sec/cm

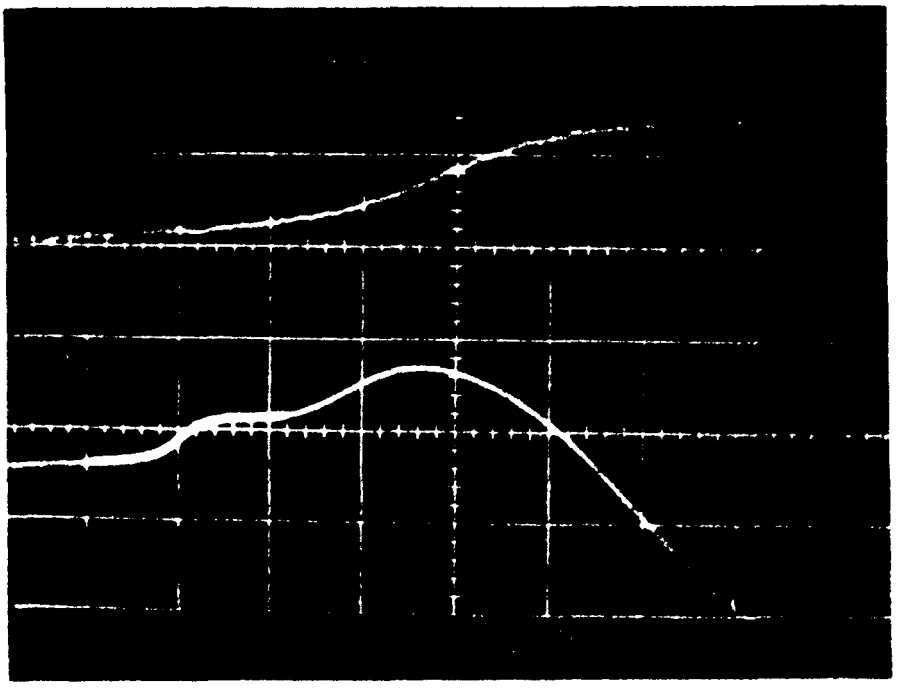

Fig. 16. **Pressure profile for a reflecting shock wave where:**

Incident shock Mach no.: $M_s = 7.40$
Driven gas: Argon at 30 μ Hg
Pressure jump: $\Delta P = 11.8$ mm Hg
Gauge voltage: V = 4.0 kV
Upper trace: .02 v/cm, 1 μ sec/cm
Lower trace: .05 v/cm, 5 μ sec/cm

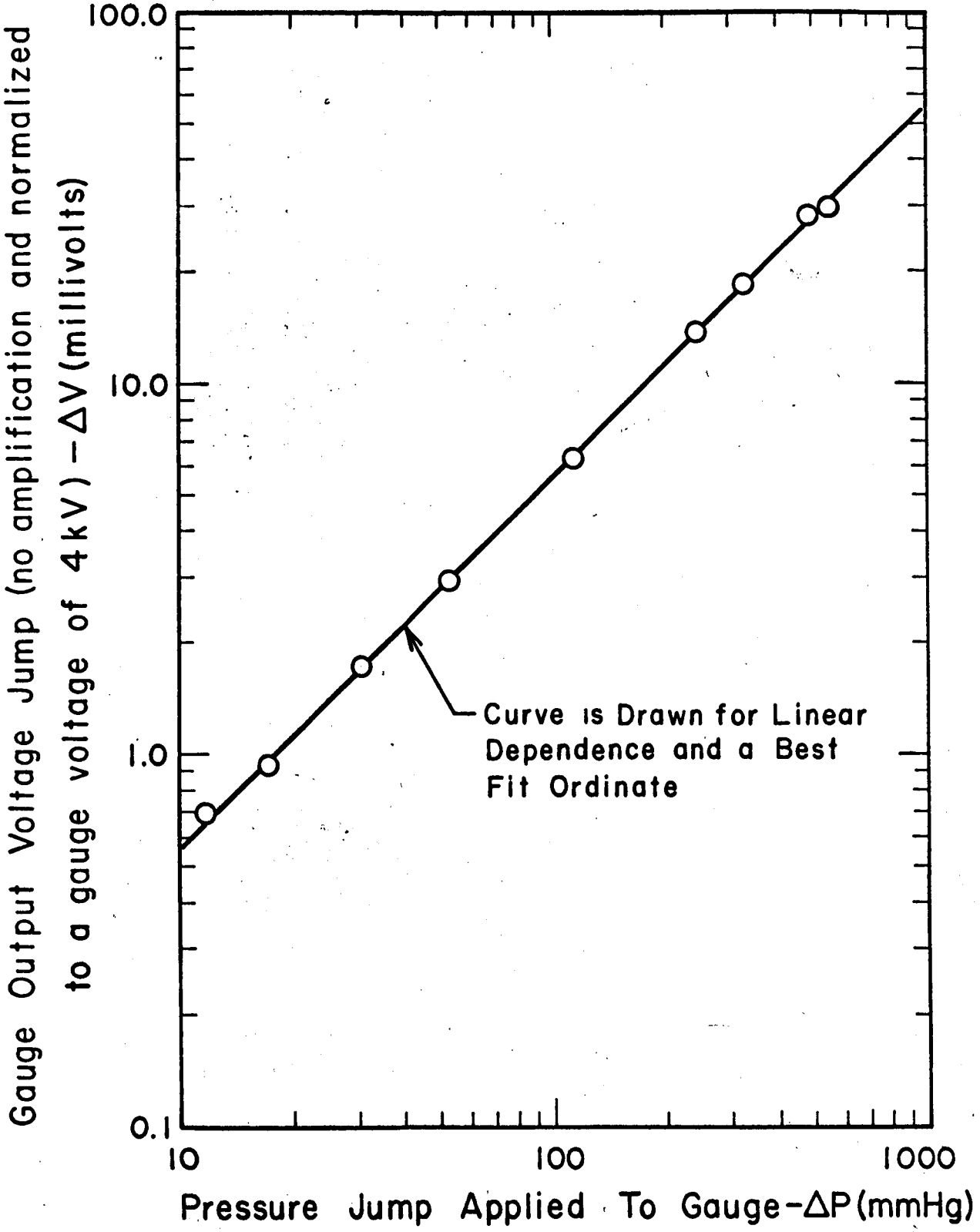

FIG. 17.
D. BAGANOFF
REV. SCI. INSTR.